Switchable Metasurface Absorber Used for Enabling Reconfigurable Power Angular Spectrum in Reverberation Chamber

Qingqing Zhang[1], Zhenzhen Zhao[2], Binhui Liu[3], Wei Xue[4], Xiaoming Chen[1], Junhao Zheng[1], Hongyu Shi[1], Jianjia Yi[1] and Yi Huang[2]

[1] The School of Information and Communications Engineering, Xi'an Jiaotong University, Xi'an, China
[2] The Department of Electrical Engineering and Electronics, University of Liverpool, Liverpool, UK
[3] The 5th Electronic Research Institute, Ministry of Industry and Information Technology, Guangzhou, China
[4] The School of Electronics and Information, Northwestern Polytechnical University, Xi'an, China

E-mail: xiaoming.chen@mail.xjtu.edu.cn

Received xxxxxx
Accepted for publication xxxxxx
Published xxxxxx

Abstract

The reverberation chamber (RC) provides a fast and repeatable method for over-the-air (OTA) testing of wireless devices. Moreover, the RC-based method can reduce the OTA testing cost to a great extent. But the defect of the RC is also obvious. Compared to a multi-probe anechoic chamber, the channel spatial characteristics in RC are uncontrollable. The device under test in a RC usually sees a statistically isotropic channel and there is a strong impediment to control the channel in RC, which constrains the RC's OTA applications. In this paper, we propose a method to realize reconfigurable RC enabling arbitrary channel power angular spectrum (PAS) by using a switchable metasurface absorber. Specifically, the unit cell of the metasurface can be switched between the reflection and absorption states by providing different bias voltages. By mounting the switchable metasurface absorber on the RC's inside walls, the boundary conditions of the RC in the covered area could be switched electronically. Consequently, the channel's PAS can be controlled by changing the local states of the switchable metasurface absorber. As a proof of concept, a prototype of the switchable metasurface absorber is made and comprehensive experiments are conducted to verify the effectiveness of the switchable metasurface applied to enable reconfigurable PAS in RC.

Keywords: absorber, metasurface, over-the-air (OTA) testing, power angular spectrum, reverberation chamber

1. Introduction

The multiple-input and multiple-output (MIMO) techniques have been adopted in communication systems to increase data rates [1], which also brings challenges to the over-the-air (OTA) testing of multi-antennas. Several OTA testing solutions have been proposed in [2]-[7] to evaluate the performance of multi-antennas. These testing methods are mainly categorized into two groups, e.g., the anechoic chamber-based methods and the RC-based methods. In the multi-probe anechoic chamber, the channel spatial characteristics can be controlled by the probe power weightings [3]. Nevertheless, a large number of probes are

needed to ensure accurate channel emulation, which leads to a high cost. Compared to the anechoic chamber, the RC provides a more compact and cost-effective solution for OTA testing. But the field distribution in a well-stirred RC is usually spatially uniform and isotropic [8]. It is hard to control the RC's channel spatial characteristics.

As a result, increasing attention is focused on how to control the channel spatial characteristics and realize arbitrary channel power angular spectrum (PAS), i.e., the angular dependence of the power spectrum, in the RC. Up to now, few researches have been conducted to achieve this goal.

In the loaded RC proposed in [9]-[12], the statistically isotropic property of the channel can be altered by adding absorbing materials. Non-uniform PAS can be realized and qualitatively predicted by loading the RC with absorbing materials. Nevertheless, these methods are confined to the channel with fixed PAS. To fully test the adaptive beamforming performance of the MIMO device [13], the emulated channel in the testing environment needs to be dynamic with reconfigurable PAS.

Another method is the reconfigurable RC proposed in [14], and [15]. The reconfigurable RC is a metal cavity with many probes mounted on its side walls. By tuning the excitations and termination impedances of the probes, the field distribution can be dynamically controlled. Yet, the optimization and tuning of the reconfigurable chamber to get the required field distribution is rather complex; and the focus of these works is on controlling the field distribution instead of the PAS.

Different from the reconfigurable RC based on probes, the reconfigurable RC proposed in this work is based on a switchable metasurface absorber. Recently, switchable metasurface absorber has been widely proposed in energy harvesting [16], [17], polarization manipulation [18], wave-field shaping [19], refractive index sensing [20], precise localization [21], sensor [22], and microwave imaging [23]. In addition, the metasurface is also used to improve the uniformity of fields in RC [24], and tune the coherence bandwidth of RC [25]. In this work, an electronically switchable metasurface absorber is applied to dynamically control the RC's PAS. By resorting to the switchable metasurface, the channel's PAS can be dynamically reconfigured and the spatial characteristics of the channel can be controlled in a straightforward way. Due to the electronically switchable working states of the metasurface unit cells, dynamic spatial channel control is enabled.

Sevaral switchable metasurface absorbers have been proposed in previous works [25]-[28]. However, the bandwidth of switchable metasurface absorber proposed in [26] is ultrathin. The relatively wideband switchable absorbers proposed in [25], [27], [28] are less flexible in their switchable ability. The switchable absorber in [25] is only switchable for the incident waves with matched polarization. In [27], significant power of incident waves have been absorbed when the wideband metasurface switched to reflection state. In [28], the metasurface have good performance at reflection state, but the maximum absorption rate of the metasurface is only about 85%. Consequently, the metasurface designed in this paper try to make a tradeoff between bandwidth and switchable ability for reconfigurable RC application. And the proposed metasurface have a good performance on its switchable ability.

In this paper, Section II elaborates on the design, simulation, and measurement of the metasurface. Section III demonstrates the reconfigurable PAS achieved in RC via the switchable metasurface absorber. Finally, the conclusions of this work are drawn in Section V.

2. Switchable metasurface absorber

2.1 Design of the structure

Due to the randomly distributed fields in RC, the performance of the metasurface absorber needs to be polarization-insensitive and angle-insensitive. Moreover, the amplitude of the reflection coefficient of the metasurface should be above -1 dB in the reflection state, while its amplitude should be under -10 dB in the absorption state within the operating band in order to clearly distinguish the two states in the RC.

The final geometry of the switchable metasurface element is illustrated in Fig. 1.

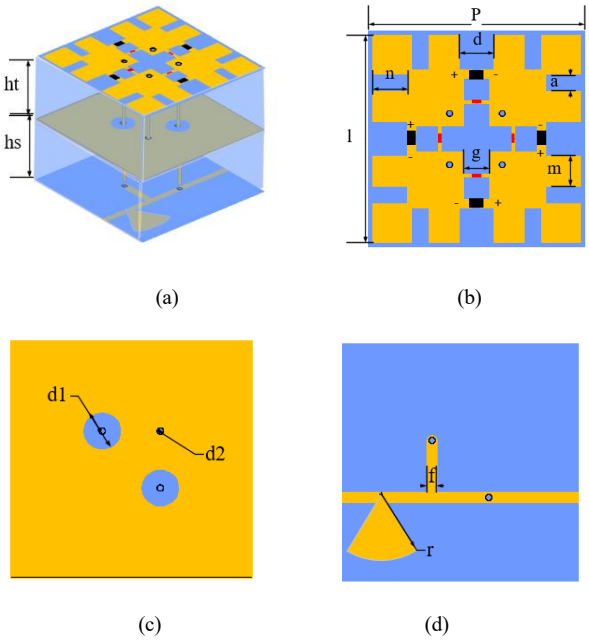

Fig. 1. Geometry of the proposed switchable metasurface absorber. (a) Perspective view. (b) Top metallic layer. (c) Second metal layer. (d) Bottom metal layer.

Fig. 1 (a) gives the perspective view of the unit cell. There are three metal layers and two substrate layers in the structure. The metal layer (in yellow color) is made of copper with a conductivity of $\sigma = 5.8 \times 10^7$ S/m. The two substrate layers (in

blue color) are FR4, with a relative dielectric constant of ε_r = 4.4 and a loss tangent δ = 0.002. The two substrate layers have the thicknesses *ht* = 4 mm and *hs* = 0.5 mm, respectively. (Note that in order to illustrate the structure clearly, the substrates shown in Fig. 1 (a) are much thicker than their real thicknesses.) The top metal layer plays a major role in the switchable metasurface absorber. The metallic structure in the top layer can be seen as a cross slot in the middle and four E-shaped slots around as presented in Fig. 1 (b). The PIN diodes (SMP1345-079LF) are denoted in black color and chip resistors (200 ohms) are represented in red color.

The second metal layer works as a metal ground and connects to the negative ports of the PIN diodes through blind vias. And the two circle slots in this layer as presented in Fig. 1 (c) are to isolate the metal ground from through vias. The third metal layer is designed to provide a bias voltage to the positive ports of the diodes through vias. In Fig. 1 (d), the copper line connects the two through vias in a unit cell and extends to the adjacent unit cell. In this way, each row of the metasurface can be controlled independently. And the fan-shaped stub is used to decouple the RF from the DC. The PIN diodes on the top metallic layer can be switched on and off by applying a bias voltage to them. Thus, the working state of the metasurface unit cell could be switched electronically. The optimized parameters of the structure are shown in Table I.

TABLE I

VARIABLE VALUES OF METASURFACE ABSORBER

Symbol	*P*	*l*	*n*	*m*	*d*	g	a
Value (mm)	25.0	24.0	4.0	3.5	4.0	3.0	2.0
Symbol	*d2*	*d1*	*f*	*ht*	*hs*	*r*	
Value (mm)	0.6	6.0	1.0	4.0	0.5	8.7	

To further explain the proposed structure, the evolution of the metallic pattern on the top layer are presented. Fig. 2 shows the structures and their reflection coefficients under different incident angles in transverse electric (TE) mode. Structure I in Fig. 2 (a) has a thin absorption band with polarization-insensitive and angle-insensitive performances. In structure II, four resistors are added to the structure, and the bandwidth is broadened to cover the important 5G band (3.3 - 3.8 GHz) as shown in Fig. 2(b). However, there is an unwanted oscillation near the operation band. Based on structure II, some slots are added to the structure as shown in Fig. 2 (c). The frequency response of the metasurface become more stable. Moreover, the phase shifts of the reflection coefficients under large incident angles in TE mode are decreased. More detailed simulation results of proposed structure are presented in the next subsection.

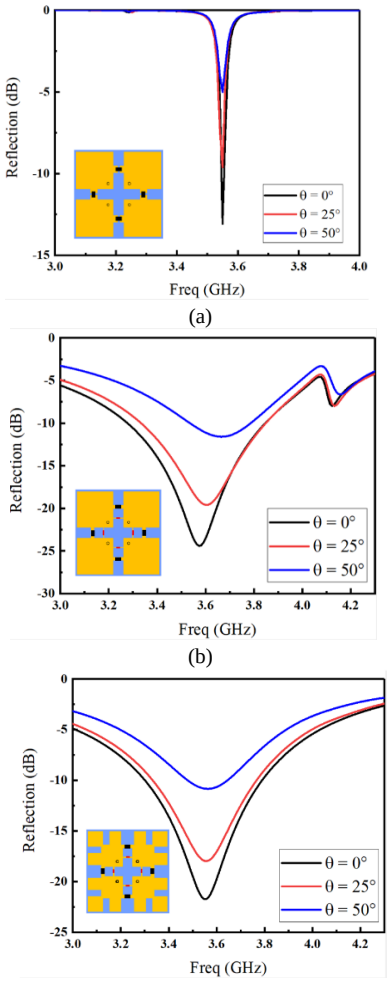

Fig. 2. Design evolutions and their reflection coefficients under different incident angles in transverse electric (TE) mode. (a) Structure I. (b) Structure II. (c) Proposed structure.

2.2 Simulation

The switchable metasurface absorber is simulated with unit cell boundaries in CST Microwave Studio. The operating bandwidth of the switchable metasurface is from 3.3 GHz to 3.8 GHz, covering the important 5G band. The metasurface works as an absorber and reflector when switched off (i.e., with 0-V bias voltage) and on (i.e., with 1-V bias voltage), respectively. The reflection coefficients and absorption rates of the metasurface under the two states are presented in Fig. 3. The absorption rate is defined as the ratio of absorbed power to incident power, which can be calculated by subtracting the power of reflected and transmitted waves from the incident power. Since there exists a metal ground layer in the metasurface structure, the transmitted waves can be neglected. Fig. 3 (a) and (b) present the reflection coefficients of the metasurface under different incident angles and polarizations.

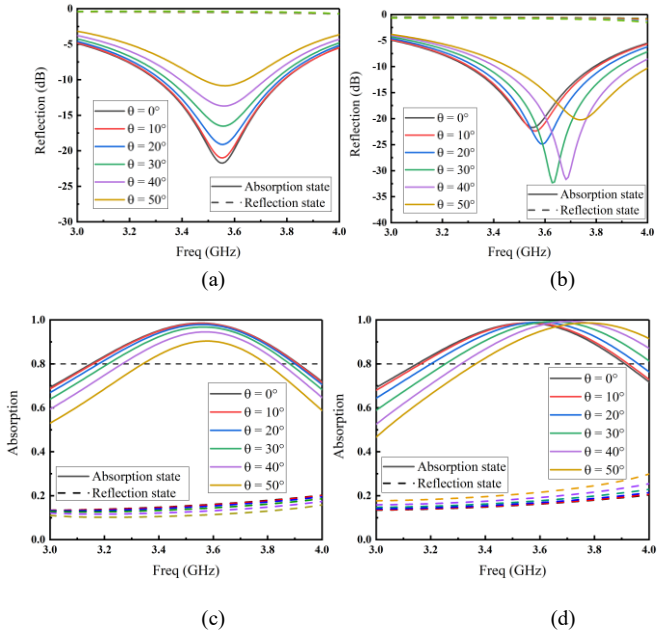

Fig. 3. Simulated results of the switchable metasurface under different incident angles and polarizations. (a)Reflection in TE mode. (b) Reflection in TM mode. (c) Absorption in TE mode. (d) Absorption in TM mode.

Fig. 3 (c) shows the absorption rates of the metasurface under different incident angles in TE mode. The absorption rates of the metasurface in absorption state are presented by solid lines, while the absorption rates in the reflection state are denoted in dotted lines. It can be seen that the absorption rate is above 90% from 3.3 GHz to 3.8 GHz at normal incidence in the absorption state, and the maximum value reaches 98.5%. With the incident angle increasing, the absorption rate is slightly reduced, but it still maintains around 80% when the angle is up to 50°. While in the reflection state, the majority of the incident power has been reflected, and the absorption rates are around 15%. Fig. 3 (d) gives the absorption rates under different incident angles in transverse magnetic (TM) mode. From Fig. 3, it is concluded that the absorption rates of metasurface can remain quite stable both in TE and TM modes until the incident angle is up to 50°. Table II compares the performance of the proposed switchable metasurface with that of the previous switchable absorbers.

TABLE II

PERFORMANCE COMPARISONS BETWEEN THE PROPOSED WORK AND PREVIOUS ONES

	Working band	**Absorption range**	**NLE**	**Polarization**
[25]	2.3-2.5 GHz (8.3%)	10%-99%	2	single
[26]	2.33-2.4 GHz (3%)	2%-99%	8	dual
[27]	4.9-12.6GHz (88%)	50%-99%	6	dual
[28]	2.2-2.4 GHz (8.7%)	10%-85%	6	dual
This work	3.3-3.8 GHz (14%)	10%-98%	8	dual

Note: The working band is defined as the bandwidth with a reflection under -10 dB at absorption state, absorption range is the range of the absorption rates between different work states, NLE is the number of lumped elements in a unit cell.

2.3 Analysis

To have a better insight into the working mechanism of the switchable metasurface, the surface current distribution (when the electric field at normal incidence) of the top layer at resonant frequency is presented in Fig. 4. Compared to reflection state, in absorption state, there is strong resonant current on the top layer. The surface current is trapped in the middle area, and mostly trapped in the resistors when the PIN diodes switch off. So, the energy of incident waves can be dissipated by the resistors. While in reflection state, more weak surface current is inspired by the incident waves. And majority of the surface current flow through the PIN diodes with negligible ohmic loss instead of the resistors, resulting in low absorption rates and high reflection coefficients.

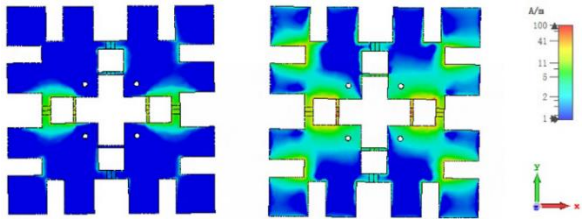

Fig. 4. Surface current distribution of the switchable metasurface at 3.55 GHz. (a) Reflection state. (b) Absorption state.

The corresponding equivalent circuit model (ECM) of the structure is also presented in Fig. 5(a). The corresponding ECM is a two-port network. Z_0 is the free-space wave impedance. The top metallic layer in the metasurface structure is equivalent to the circuit in the blue dotted box. The substrate layer in the structure is modeled by the transmission line with specific characteristic impedance Z_a in the ECM. The via holes and feeding network of the structure are neglected in the EMC model. The top metallic layer in the metasurface consists of periodic unit cells and the unit cells are symmetric structures. As presented in Fig. 5(b), the unit cell of the metasurface is composed of four identical symmetric structures as denoted in the red dotted box. As shown in Fig. 5(b), the gaps in the structure are equivalent capacitances and the metal strips in the structure are equivalent to inductances. The equivalent lumped elements corresponding to particular physical structure is noted in Fig. 5(b). Moreover, the chip resistor is equivalent to R_b with 200 ohms. The PIN diode (SMP1345-079LF [29]) under 0 V (off state) is equivalent to a capacitance C_{off} (0.12 pF) and an inductance L_{off} (0.7 nH) in series, while under 1 V (on state), it is equivalent to a resistance R_{on} (1.5 ohm) and an inductance L_{on} (0.9 nH) in series. Finally, the complete ECM of the metasurface absorber at normal incidence is shown in Fig. 5(a).

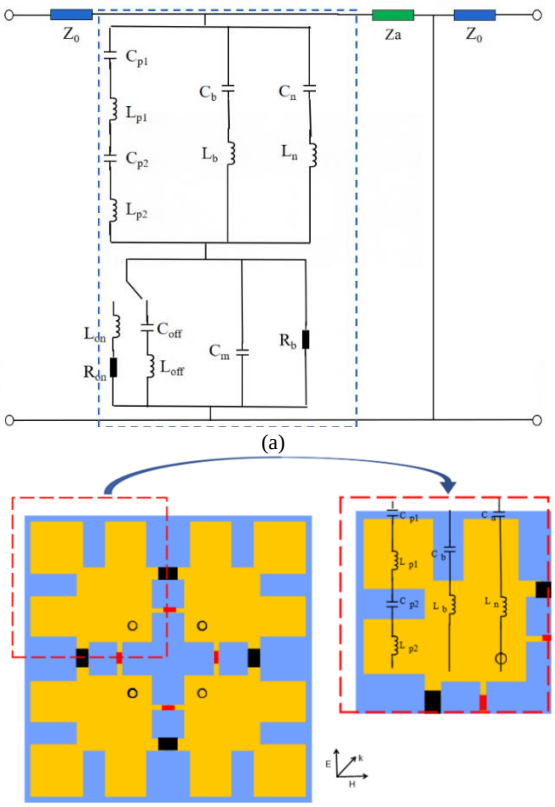

Fig. 5. (a) The ECM of the switchable metasurface absorber. (b) The physical meaning of the the equivalent lumped elements corresponding to the structure.

The work mechanism of the switchable metasurface absorber can be roughly verified by using the ECM. The variable values of the equivalent circuit model are presented in Table III. Full-wave simulation results performed in CST and the ECM results simulated in ADS are presented in Fig. 6. The reflection coefficients with the PIN diodes in the on state are denoted in blue, while they are denoted in red with the PIN diodes in the off state. The results agree well with each other.

TABLE III

PARAMETER VALUES OF THE EQUIVALENT CIRCUIT MODEL

Symbol	L_n	C_n	C_m	L_{off}	R_{off}
Value	0.77 nH	0.71 pF	0.32 pF	0.9 nH	1Ω
Symbol	L_b	C_b	L_{p2}	C_{on}	L_{on}
Value	53.31 nH	1.57 pF	55.27 nH	0.12 pF	0.7 nH
Symbol	C_{p1}	C_{p2}	L_{p1}		
Value	0.1 fF	6.94 pF	20.27 nH		

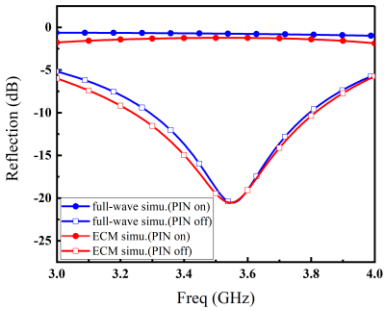

Fig. 6. Full-wave simulation and ECM simulation results of the switchable metasurface absorber.

2.4 Measurement

The switchable metasurface absorber is manufactured with an overall size of 400 mm × 400 mm, consisting 16 × 16 elements. A photograph of the prototype is shown in Fig. 7(a). The experimental setup for reflection measurements is illustrated in Fig. 7(b). As shown in Fig. 7(b), a pair of horn antennas mounted on two mechanical arms are adopted as transm itting and receiving antennas, respectively. The distance from the horn antennas to the switchable metasurface is 2 m. Meanwhile, the metasurface is placed in the center of the platform with absorbing material surrounded to avoid diffraction from its surroundings. In addition, a copper plate with a size of 400 mm × 400 mm (the same size as metasurface) is used for calibration to avoid environmental error. The rotation angle θ of the mechanical arms [cf. Fig. 7(b)] can be precisely controlled by a computer. The reflection coefficients of the proposed metasurface under different incident angles can be obtained by sweeping θ, and the reflection under different polarizations can be gathered by rotating the horn antennas to change the polarization of incident waves.

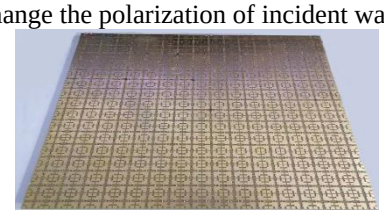

(a)

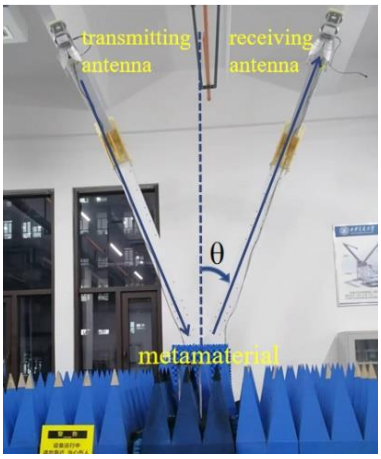

(b)

Fig. 7. Photos of (a) the prototype consisting of 16 × 16 units and (b) measurement setup of the prototype in the laboratory.

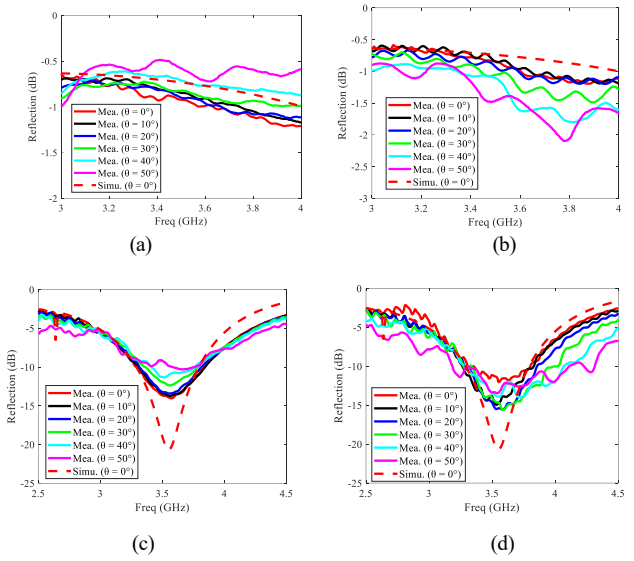

Fig. 8. Measured reflection coefficients of the switchable metasurface in (a) reflection state for TE mode, (b) reflection state for TM mode, (c) absorption state for TE mode, and (d) absorption state for TM mode.

The measured results are presented in Fig. 8. In the reflection state, the measured reflection coefficients for TE mode and TM mode are shown in Figs. 8 (a) and (b), respectively. Amplitudes of the reflection coefficients are around -1 dB under different polarizations and incident angles. In the absorption state, the measured reflection coefficients for TE mode and TM mode are shown in Figs. 8 (c) and (d), respectively. Amplitudes of the measured reflection coefficients are under -10 dB from 3.3 GHz to 3.8 GHz, showing that most power of the incident wave is absorbed by the metasurface. It can be also found that the reflection curves remain rather stable under different polarizations and incident angles, indicating the metasurface can work under a wide-angle range of the incident waves. The dotted lines in Fig. 8 are the simulated reflection coefficients at normal incidence for comparison.

3. Measurements of reconfigurable PAS in RC

In this section, further experiments are conducted in an RC loaded with the switchable metasurface absorber to verify the realization of reconfigurable PAS.

The schematic of the RC measurement setup is shown in Fig. 9 (a). The RC has a size of 1.50 m × 1.44 m × 0.92 m. There are two rotating mechanical stirrers and a turn-table platform in the RC. A pair of horn antennas are used as receiving and transmitting antennas. The transmitting antenna is fixed on the rotating platform and the receiving antenna is placed in the corner of RC. The rotating radius (defined as the distance between the center of the rotating platform and the transmitting antenna) is denoted as *r*. Both antennas are connected to a vector network analyzer (VNA).

A prototype of the switchable metasurface absorber is mounted on a side wall of RC. A photograph of the measurement environment inside the RC is shown in Fig. 9 (b).

Different from an unloaded and well-stirred RC, the field distribution in RC can become non-uniform when the absorbing material is employed. Specifically, the PAS experiences a significant reduction in the angular coverage of absorbing metasurface. Thus, when the RC is loaded with the switchable metasurface absorber as shown in Fig. 9, the PAS within the angular range covered by the metasurface (about 70° to 110°) can be reconfigured by switching ON and OFF of the unit cells of the metasurface. Obviously, the range of the reconfigurable PAS can be extended by placing more of such a metasurface in the RC. When all the side walls of the RC are covered by the switchable metasurface absorber, the PAS over the whole angular range can be reconfigured. Nevertheless, since this work focuses on the reconfigurable PAS in the RC loaded with the switchable metasurface, for the proof-of-concept only one switchable metasurface is used and it suffices to demonstrate the effectiveness of the proposed switchable metasurface if a reconfigurable PAS is realized in such an angular region.

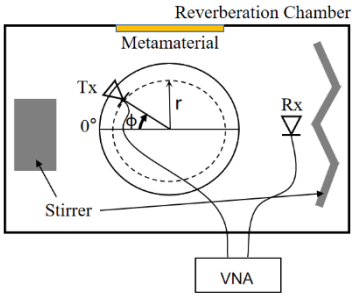

(a)

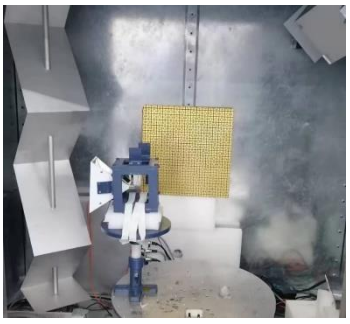

(b)

Fig. 9. (a) Schematic diagram and (b) photo of the measurement setup with switchable metasurface.

The RC's PAS is analyzed and obtained by using the method presented in [30]. The PAS in RC is analysed and obtained from the S-parameter S_{21} between the transmitting and receiving antennas collected by VNA. The S_{21} is collected when the rotating platform rotates 360° with an azimuthal interval of 1°. The collected S_{21} which relevant to signal frequency, rotating radius and azimuth angle can be expressed as channel transfer function $h^{(n)}(f, r, \phi)$. Where *n* is the number of mechanical stirrings.

Then the Fourier transform of the channel transfer function is obtained as

$$H^{(n)}(f,k,\phi) = \left| \int h^{(n)}(f,r,\phi) e^{jkr} dr \right|^2 \quad (1)$$

k is the wave number, the power angular spectrum containing overall multipath components in the RC can be calculated by integrating k as follows

$$H^{(n)}(f,\phi) = \int_0^{k_0} H^{(n)}(f,k,\phi) dk \quad (2)$$

k_0 is the wave number in free space. Then the power angular spectrum $H^{(n)}(f, \phi)$ characterizes the received power as function of frequency and azimuth angle is obtained. The channel transfer function $h^{(n)}(f, r, \phi)$ is proportional to the reflectivity of metasurface. And $H^{(n)}(f, \phi)$ is proportional to the square of the reflection coefficients of the metasurface.

The PASs under five different mechanical stirs are measured and averaged over the operation band. The averaged PASs in the reflection and absorption states of the metasurface are presented in Fig. 10. When all unit cells of the switchable metasurface are in the reflection state, the PAS in RC is statistically uniform as denoted by the blue line in the plot. When the whole metasurface is set to the absorption state, the power density between 70° to 110° is reduced as expected. Note that the incident waves from the ceiling, floor, and upper and lower parts of the uncovered sidewall all contribute to the power density. Hence, the power density will be further reduced when these parts are covered by the metasurface.

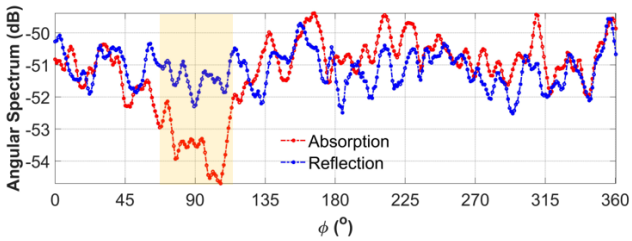

Fig. 10. PAS in the RC loaded with the switchable metasurface absorber.

The experiment verified roughly the control of the power angular spectrum in RC. Since every column of the metasurface elements can be controlled independently, a more precisely reconfigurable PAS can be realized to enable an arbitrary channel model. In addition, for better comparison, an RF absorber is placed on the left side of the metasurface and the rest of the inner walls remain uncovered. A photograph of this configuration is shown in Fig. 11.

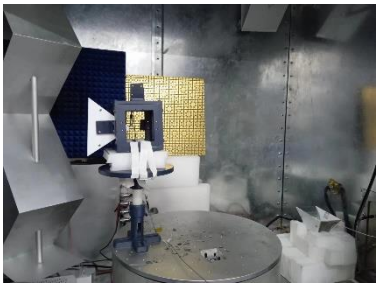

Fig. 11. Photo of the measurement setup with switchable metasurface and conventional absorber.

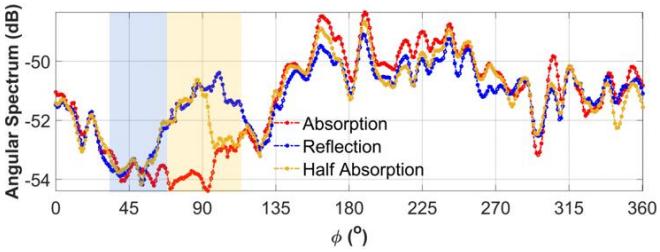

Fig. 12. PAS in the RC loaded with switchable metasurface absorber and RF absorber.

Similarly, the PASs under different work states of the metasurface are shown in Fig. 12. The blue and yellow block in the plot indicates the angle range covered by RF absorbers and metasurface, respectively. The blue dotted line refers to the PAS when all columns of the metasurface are in a reflection state. The blue line has an obvious increment at 70° due to the transition between RF absorber and the reflective metasurface. The red dotted line is measured when all columns are in the absorption state. By comparison of the red line in blue and yellow block covered area, it can be seen that the metasurface in the absorption state behaves as good as the RF absorbers.

While the yellow line is measured by setting the columns in the left half of the metasurface in the reflection state and the other half in the absorption state (i.e., half absorption). The yellow line coincides with the blue line within 70° to 90°, and coincides with the red line in 90° to 110°, which shows a good agreement with the working state set up of the metasurface. This implies that by switching the columns of the unit cells independently, fine control of the PAS can be achieved. Comparing the three lines in the plot, it is safe to conclude that the RC's PAS can be reconfigured by using the switchable metasurface in an efficient way.

4. Conclusions

This paper has proposed a method to enable reconfigurable PAS in RC by using a switchable metasurface absorber. To this end, a polarization-insensitive and angle-insensitive switchable metasurface absorber has been designed and fabricated. Two experiments were conducted in the RC loaded with switchable metasurface to verify that the channel special characteristics could be electronically controlled in a simple way, and arbitrary PAS in RC could be realized by setting the work states of the metasurface. By using the switchable metasurface, dynamic control of the spatial channel is enabled in the low-cost and compact RC, providing a promising method for cost-effective OTA testing of wireless devices.

Acknowledgements

This work was supported in part by the National Natural Science Foundation of China under Grant 62171362, the Key

Research and Development Program of Shaanxi under Grant 2023-YBGY-246, and in part by the Aeronautical Science Foundation of China under Grant 2022Z062053002.

References

[1] Paulraj A, Nabar R and Gore D 2003 *Cambridge University Press*.
[2] Toivanen J T, Laitinen T A, Kolmonen V M and Vainikainen P 2011 *IEEE Trans. Instrum. Meas.* **60** 1275-281
[3] Fan W et al 2013 *IEEE Trans. Antennas Propag.* **61** 84306-4314
[4] Zhang Q, Loh T H, Zhang W, Yang Y, Huang Z and Qin F, 2022 *IEEE Trans. Instrum. Meas.* **71** 6501215
[5] Yu W, Qi Y and Liu K, et al 2014 *IEEE Trans. Electromagn. Compat.* **56** 61691–1696
[6] Xue W, Li F, Chen X, Zhu S, Zhang A and Svensson T 2021 *IEEE Trans. Instrum. Meas.* **70** 1003112.
[7] Nogueira C L et al 2022 *IEEE Trans. Instrum. Meas* **71** 5503411
[8] Rajamani V, Bunting C F and West J C 2012 *IEEE Trans. Instrum. Meas.* **61** 102759-2764
[9] Becker M G, Horansky R D, Senic D, Neylon V and Remley K A 2018 *European Conference on Antennas and Propagation* 1-5.
[10] Chen Y, Zhou X, Ji J, Zhai S and Chen D 2021 *Progress In Electromagnetics Research M* **100** 117-125
[11] Otterskog M and Madsen K 2004 *Microw. Opt. Technol. Lett.* **43** 3192–195
[12] Valenzuela-Valdes J F, Martinez-Gonzalez A M and Sanchez-Hernandez D A 2008 *IEEE Antennas Wireless Propag. Lett.* **7** 325-328
[13] Fan W, Kyösti P, Romney M, Chen X, and Pedersen G F 2018 *IEEE Commun. Mag.* **56** 764-71
[14] Arnold B T and Jensen M A 2023 *IEEE Trans. Antennas Propag.* **33** 12937
[15] Arnold M D, Jensen M A and Mehmood R 2023 *IEEE Trans. Antennas Propag.* **71** 65289-5298
[16] Agrahari R et al 2023 *Microw. Opt. Technol. Lett.* **65** 82252-2261
[17] Amin M, Almoneef T S, Siddiqui O, Aldhaeebi M A and Mouine J 2021 *IEEE Antennas Wireless Propag. Lett.* **20** 102043-2047
[18] Agrahari R, Rajbhar P K, Mahto M and Jain P K 2023 *J. Appl. Phys.* **133** 094902
[19] Li X S et al 2020 J. Phys. D: Appl. Phys. **53** 195301
[20] Agrahari R, Dwivedi S, Jain P K and Mahto M 2023 *IEEE Trans. Nanotechnol.* **22** 328-335
[21] Hougne P, Imani M, Fink M, Smith D and Lerosey G 2018 *Phys. Rev. Lett.* **121** 6063901
[22] Yao Y et al 2021 *J. Phys. D: Appl. Phys.* **54** 113002
[23] Asefi M and LoVetri J 2017 *IEEE Trans. Micro. Theory Tech.* **65** 93172-3179
[24] Guo Y, Weng Z, Jiao Y, Liu L, Qi Y and Zhang H 2023 *IEEE Symposium on Electromagnetic Compatibility & Signal/Power Integrity (EMC+SIPI)* 79-82.
[25] Yi J, Dong C, Xue W and Chen X 2022 *IEEE Trans. Antennas Propag.* **70** 64908-4913
[26] Ghosh S and Srivastava K V 2016 *Electron. Lett.* **52** 131141–1143
[27] Li H, Costa F, Wang Y, Cao Q and Monorchio A 2020 *IEEE Trans. Antennas Propag.* **68** 65033-5038
[28] Li A, Kim S, Luo Y, Li Y, Long J and Sievenpiper D F 2017 *IEEE Trans. Microw. Theory Tech.* **65** 82810-2818
[29] https://www.skyworksinc.com/search?q=smp1345-079lf
[30] Zheng J and Chen X 2022 *International Symposium on Electromagnetic Compatibility – EMC Europe* 555-559